Microporous Materials Hot Paper

How to cite: *Angew. Chem. Int. Ed.* **2021**, *60*, 10806–10813
International Edition: doi.org/10.1002/anie.202100717
German Edition: doi.org/10.1002/ange.202100717

Conductive Metallophthalocyanine Framework Films with High Carrier Mobility as Efficient Chemiresistors

Yan Yue[+], Peiyu Cai[+], Xiaoyi Xu, Hanying Li, Hongzheng Chen, Hong-Cai Zhou, and Ning Huang**

Abstract: *The poor electrical conductivity of two-dimensional (2D) crystalline frameworks greatly limits their utilization in optoelectronics and sensor technology. Herein, we describe a conductive metallophthalocyanine-based NiPc-CoTAA framework with cobalt(II) tetraaza[14]annulene linkages. The high conjugation across the whole network combined with densely stacked metallophthalocyanine units endows this material with high electrical conductivity, which can be greatly enhanced by doping with iodine. The NiPc-CoTAA framework was also fabricated as thin films with different thicknesses from 100 to 1000 nm by the steam-assisted conversion method. These films enabled the detection of low-concentration gases and exhibited remarkable sensitivity and stability. This study indicates the enormous potential of metallophthalocyanine-based conductive frameworks in advanced stand-off chemical sensors and provides a general strategy through tailor-make molecular design to develop sensitive and stable chemical sensors for the detection of low-concentration gases.*

Introduction

In past decades, reticular chemistry has aroused a great deal of interest toward the development of periodically ordered frameworks using various building blocks.[1] This strategy allows the predesign of target frameworks through the rational selection of topological structures and building blocks. Among these materials, metal–organic frameworks (MOFs) and covalent organic frameworks (COFs) constitute the prime examples, which combined the advantages of intrinsic crystallinity, remarkable porosity, and high structure flexibility.[2] These crystalline materials have been widely utilized in various fields, including gas storage,[3] gas separation,[4] heterogeneous catalysis,[5] chemical sensing,[6] proton conduction,[7] optoelectronics,[8] energy storage,[9] and sewage treatment.[10] To impart special performances to these frameworks, the integration of target-oriented functional building units is generally adopted. For instance, the development of catalytic frameworks involves embedding, immobilizing, or loading catalytically active molecules, such as metalloporphyrins,[11] salen-type complexes,[12] BINAP ligands,[13] and chiral proline-based units.[14] On the one hand, the introduction of functional groups endows the frameworks with new features, greatly enhancing their structural complexity and functional diversity. On the other hand, the high crystallinity, high porosity, and high stability of these framework materials can significantly enhance the specific performance of integrated functional units. Based on these characteristic features and advantages, a great variety of functionalized MOFs and COFs are continuously being developed.

Conductive polymers are broadly utilized as an efficient platform for chemical sensing, which are generally evaluated using various microelectronic devices. The most frequently used one are chemiresistors, which are fabricated to measure the conductometric changes caused by the interaction of the polymer backbone with electronically analytes.[15] However, the development of conductive MOFs and COFs remains a major challenge because most of them lack the low-energy routes for charge transport or free charge carriers.[16] Therefore, most of these reticular frameworks behave like electrical insulators with quite low electrical conductivity ($< 10^{-12}\ S\,m^{-1}$).[17] To break through this bottleneck, two strategies have been proposed to facilitate charge transport in these materials, namely "through-bond" and "through-space" approaches.[16] Among the conductive MOFs, the 2D MOFs is a particular case of the "through-bond" approach. The extended 2D π-conjugation could greatly contribute to the improved electrical conductivity. Recently emerged conductive MOFs are developed using this approach, such as $Cu_3(HHTP)_2$,[18a] $Ni_3(HITP)_2$,[18b] and Cu_3HIB_2.[18c] The specific stacking pattern of 2D layers is similar with that in 2D COFs. The periodically ordered π-columns give rises to the self-sorted donor–acceptor arrays or bicontinuous heterojunctions at atomic precision, providing express channels for charge transportation.[19] Several examples have been established based on this structural advantage, such as 2D-NiPc-BTDA COF,[19a] DMPc-ADI-COFs,[19b] and DA-COF.[19c] Recently, a new conductive framework was successfully constructed with the Ni^{II} tetraaza[14]annulene complex as the linkage.[20] The triphenylene-based NiTAA-MOF combined the structural advantages of conductive MOFs and COFs, simultaneously possessing the metal ions and covalent

[*] Dr. Y. Yue,[+] X. Xu, Prof. H. Li, Prof. H. Chen, Prof. N. Huang
MOE Key Laboratory of Macromolecular Synthesis and Functionalization, State Key Laboratory of Silicon Materials
Department of Polymer Science and Engineering
Zhejiang University
Hangzhou, 310027 (China)
E-mail: nhuang@zju.edu.cn
P. Cai,[+] Prof. H.-C. Zhou
Department of Chemistry, Texas A&M University
College Station, TX 77843-3255 (USA)
E-mail: zhou@chem.tamu.edu
[+] These authors contributed equally to this work.
Supporting information and the ORCID identification number(s) for the author(s) of this article can be found under: https://doi.org/10.1002/anie.202100717.

bonds in the network connectivity. Upon chemical oxidation with iodine, the electrical conductivity of this material reaches up to 1 $S\,m^{-1}$ at 300 K. Inspired by this work, we designed and synthesized a metallophthalocyanine-based framework, which is fully delocalized and highly π-conjugated. This framework exhibits a high electrical conductivity up to 0.52 $S\,m^{-1}$ with a high carrier mobility up to 0.15 $cm^2\,V\,s^{-1}$. It is well-known that metallophthalocyanines are widely utilized as functional units for the preparation of efficient chemiresistors.[21] Therefore, the framework can be fabricated as thin films and utilized as a high-efficiency chemiresistive sensor for different gases.

Results and Discussion

Synthesis and Characterization of NiPc-CoTAA

In this study, the metallophthalocyanine-based framework was synthesized under typical solvothermal conditions using nickel octaaminophthalocyanine ($NiPc[NH_2]_8$), tetramethoxypropane (TMP), and cobalt acetate tetrahydrate as substrates (Scheme 1). The synthesis was carried out under a basic condition with triethylamine as catalyst at 120 °C for 5 days. The resulting 2D NiPc-CoTAA framework consisted of nickel phthalocyanines as knots and cobalt tetraaza[14]annulenes as linkers (Figure 1a,b). It was obtained as a black powder in a good yield of 78% after rinsing with various solvents in Soxhlet extractor. The cobalt tetraaza[14]annulene model complex was also synthesized and obtained as single crystals. The model complex is completely planar, facilitating the formation of closely aggregated 2D layers (Figure S1). The crystalline structure of the NiPc-CoTAA framework was resolved by its powder X-ray diffraction (PXRD) patterns in combination with theoretical simulation. It exhibited a series of PXRD patterns at 4.90°, 6.96°, 9.82°, and 25.62°, which can be attributed to the (100), (200), (300), and (001) facets, respectively (Figure 1c). The Pawley refinement generates a set of PXRD patterns, which are close to the experimental results. The structural simulation based on the P4/MMM space group offers a set of lattice parameters, namely $\alpha=\beta=\gamma=90°$, $a=b=18.0195$ Å, and $c=3.4815$ Å (Table S1). The AA stacking mode (Figure 1d) produces a sequence of diffraction peaks, which corresponds well with the experimentally observed PXRD results. On the contrary, the diffraction peaks derived from the AB stacking mode (Figure 1e) deviate a lot with the experimental patterns. The adjacent layer distance was determined as 3.48 Å, which was similar to those of other 2D COFs and MOFs.[18,19]

To investigate the property of 2D NiPc-CoTAA, it was unambiguously characterized using a variety of analysis methods. In the Fourier transform infrared (FTIR) spectrum, the appearance of a strong vibration band at 1596 cm^{-1} revealed the formation of Co^{II} tetraaza[14]annulene (Figure S2). Field emission scanning electron microscopy (FE-SEM) image indicated it adopted an irregularly granular morphology with a size around 54 μm (Figure S3). Energy dispersive X-ray (EDX) mapping analysis demonstrated that

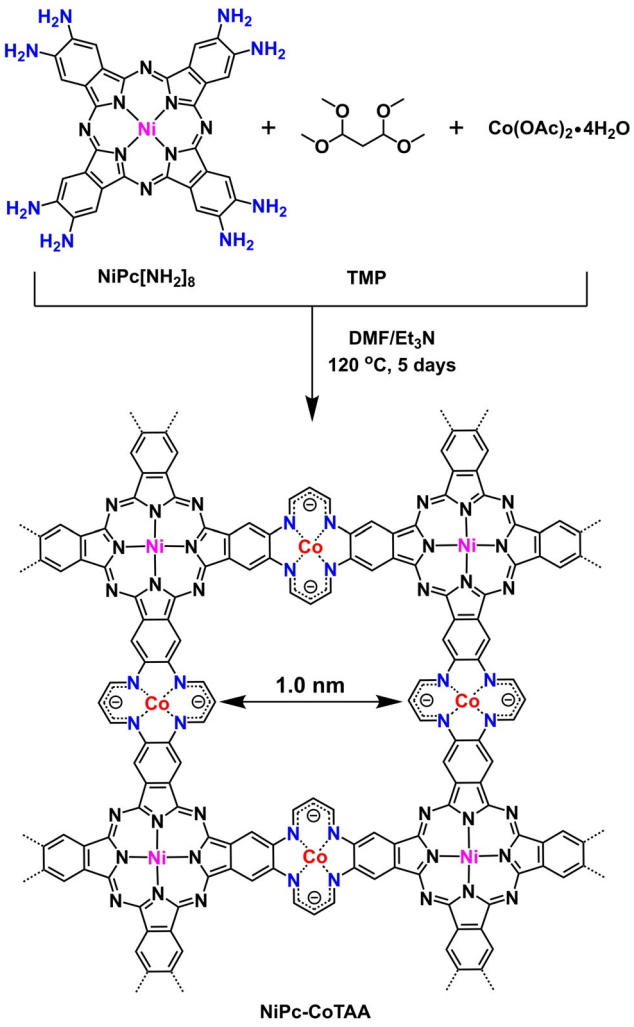

Scheme 1. Synthesis of NiPc-CoTAA using $NiPc[NH_2]_8$, TMP, and $Co(OAc)_2{\cdot}4H_2O$ under solvothermal conditions. DMF = *N*,*N*-dimethylformamide.

the elemental composition of 2D NiPc-CoTAA was in high accordance with its theoretical values (Figure S4, Table S2). High resolution transmission electron microscopy (HR-TEM) image supplies direct viewing of tetragonal pores and exhibited obvious lattice fringes with a characteristic spacing distance around 1.0 nm (Figure S5). Thermogravimetric analysis (TGA) showed this framework was thermally stable up to 450 °C under nitrogen atmosphere (Figure S6). The chemical composition of 2D NiPc-CoTAA was investigated using X-ray photoelectron spectroscopy (XPS). A series of resonance peaks of C, N, O, Ni, and Co were found in the spectrum (Figure S7). The existence of the O signal can be attributed to the H_2O molecules trapped in the porous framework or coordinated H_2O to Co or Ni metal centers. For example, four characteristic peaks at 781 and 796 eV were ascribed to Co $3d_{3/2}$ and Co $3d_{2/1}$, respectively. The other two signals at 786 and 803 eV were attributed to Co $3d_{3/2}$ and Co $3d_{2/1}$ satellite peaks, respectively (Figure 2a). These results indicated all the Co species in the NiPc-CoTAA network had a valence of +2 instead of other valence states. At the same time, the XPS

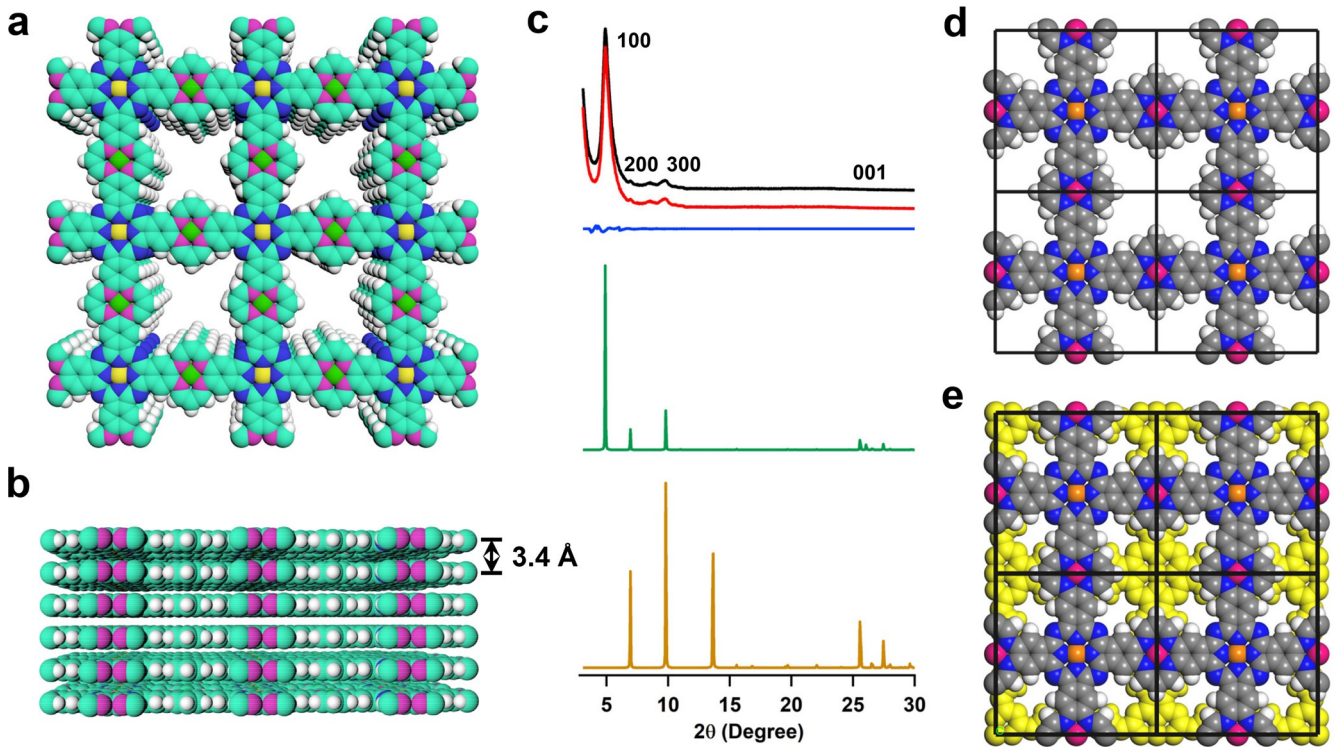

Figure 1. a) Top view and b) side view of the 2D crystalline NiPc-CoTAA framework. c) PXRD patterns of NiPc-CoTAA (black curve, experimental; red curve, simulated; blue curve, difference between experimental and simulated curves; green curve, AA stacking; brown curve, AB stacking). Unit cells of the d) AA and e) AB stacking mode (H white, C gray, N blue, Ni orange, Co red).

spectrum of Ni exhibited two characteristic signals at 856 and 874 eV, which were assigned to the Ni $3d_{3/2}$ and Ni $3d_{1/2}$ electrons, respectively (Figure S8). The other weak signals at 862 and 880 eV were assigned to Ni $3d_{3/2}$ and Ni $3d_{1/2}$ satellite peaks, respectively. This analysis result indicated two valence states of Ni existing in the NiPc-CoTAA framework, namely Ni^{II} and Ni^{0}. The molar ratio was calculated as 86/14 of Ni^{II} to Ni^{0}. The appearance of Ni^{0} is possibly due to the reducibility of Et_3N during the solvothermal process. The sample was dispersed in aqueous HCl (6 M) solution for 3 days. However, no obvious Ni^{0} particles were observed in HR-TEM (Figure S9), EDX (Figure S10), and XPS spectra (Figures S11 and S12). It is speculated that a small portion of Ni^{0} might exist as defects or single atoms instead of nanoparticles in the framework. Furthermore, the porosity of the NiPc-CoTAA framework was evaluated using nitrogen sorption measurement at 77 K. It exhibited a type-I sorption isotherm (Figure S13), which is a characteristic curve of microporous materials. The Brunauer–Emmett–Teller (BET) surface areas of NiPc-CoTAA was calculated as 186 $m^2 g^{-1}$. The pore size of NiPc-CoTAA was estimated around 0.9 nm (Figure S14), which coincided well with the theoretical value (1.0 nm).

Chemical Stability

The chemical stability of 2D NiPc-CoTAA framework in different solvents was evaluated using the intensity of PXRD peaks. After soaking in hexane, methanol, water, DMF, HCl (1 M), and NaOH (1 M) aqueous solutions overnight, NiPc-CoTAA retained its high crystallinity with almost unchanged diffraction positions and intensity (Figure S15). In addition, the residual weight of the soaked NiPc-CoTAA samples was investigated to determine their weight loss. Notably, the residual weight percentages were calculated as 100 %, 99 %, 100 %, and 98 % for the soaked samples in hexane, methanol, water, and DMF, respectively (Figure S16). In comparison, the residual proportion was determined as 96 % and 93 % after soaking in HCl (1 M) and NaOH (1 M) solutions, respectively. The results demonstrated that the Co^{II} tetraaza-[14]annulene linked framework possessed high chemical robustness under certain conditions, benefiting from the remarkable stability of tetraaza[14]annulene linkage and the accumulated 2D layer structures.

Electronic Band Diagram

The extended π-conjugation across the framework could render NiPc-CoTAA promising as an organic semiconductor or conductor material (Figure 2 b). As shown in Figure 2 c, the electronic band structure of NiPc-CoTAA monolayer was investigated using DFT calculation. The conduction band (CB) and valence band (VB) in the framework is nearly dispersionless, demonstrating the charge transport in the monolayer plane is void. The band gap for NiPc-CoTAA is calculated as 0.86 eV. The computed result through space

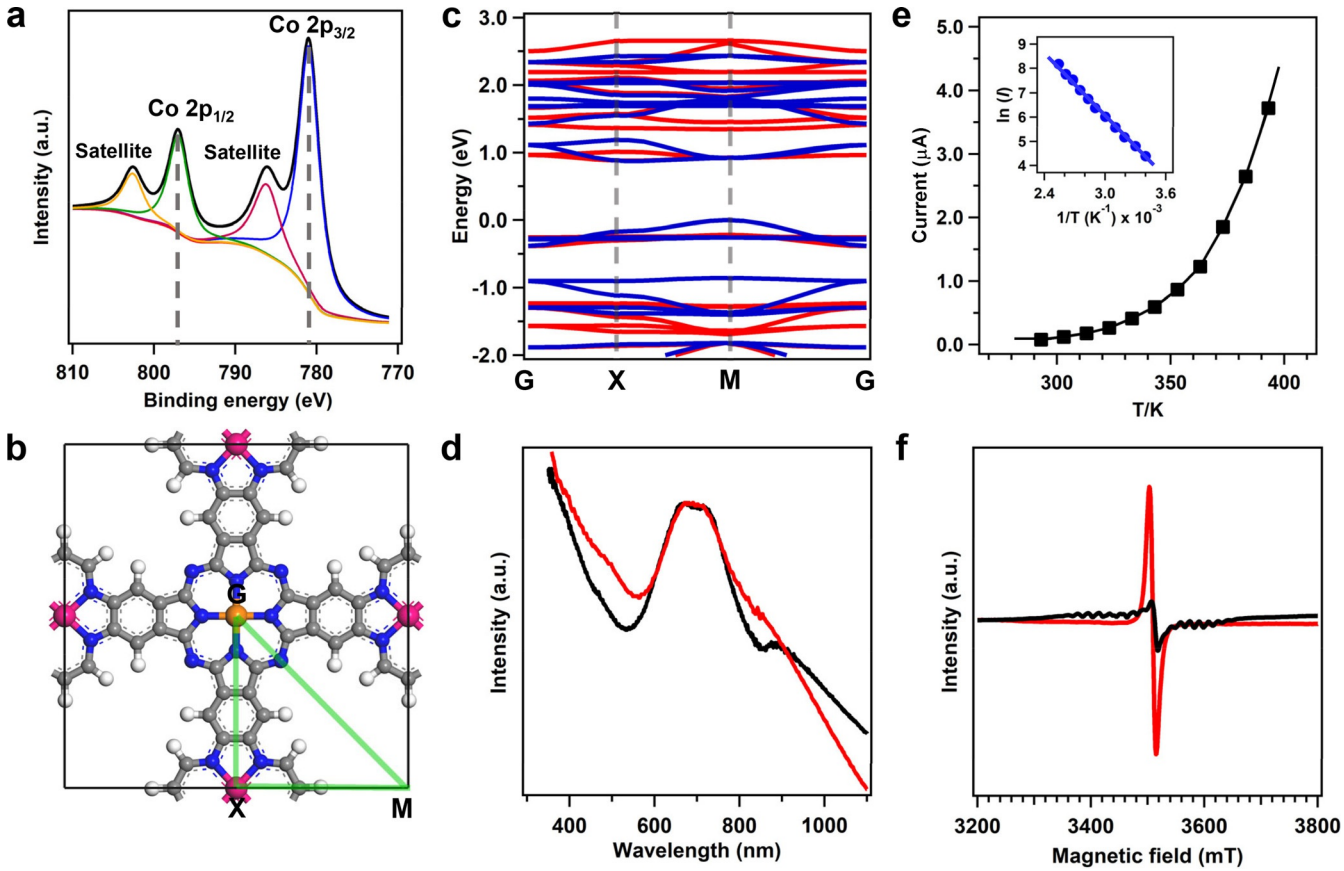

Figure 2. a) XPS spectrum of the cobalt species in the NiPc-CoTAA framework. b) Unit cell of NiPc-CoTAA and its first Brillouin zone. c) Calculated electronic band structure of NiPc-CoTAA. d) Electronic adsorption spectrum of NiPc-CoTAA (black curve) and iodine-doped NiPc-CoTAA (red curve). e) Temperature-dependent current plot of a pressed NiPc-CoTAA pellet measured by a four-point probe at temperatures from 293 to 393 K with an applied voltage of 1 V. The inset exhibits the Arrhenius plot of the current versus temperature. f) EPR spectrum of NiPc-CoTAA (black curve) and the iodine-coped NiPc-CoTAA framework (red curve).

charge transport property is consistent with those found in other phthalocyanine- and porphyrin-based COFs,[11c,22] which exhibited high carrier mobility along the direction of the stacking due to the formation of periodic π-columns. In addition, NiPc-CoTAA exhibited a broad electronic adsorption band up to 1100 nm with the maximum adsorption peak at 702 nm, confirming the 2D NiPc-CoTAA had a very low band gap around 0.86 eV (Figure 2d).

Electrical Conductivity

The Hall effect measurement was conducted to evaluate the electrical conductivity of NiPc-CoTAA. It was determined as a p-type semiconductor with a charge carrier density of 2.14×10^{13} cm^{-3} and a carrier mobility of 0.15 $cm^2 V s^{-1}$. The mobility of NiPc-CoTAA ranks as one of the highest values and is comparable with those of several landmark COF and MOF semiconductors (Table S3).[18–20] Furthermore, its conductivity was evaluated using the four-point probe measurement on a pressed powder pellet. The DC (bulk) conductivity was determined as 8.16×10^{-3} $S m^{-1}$ at 298 K. Its activation energy was calculated as 0.33 eV based on the temperature-dependent Arrhenius curve (Figure 2e). It is well-known that the metal tetraaza[14]annulene units can be partially oxidized by iodine, giving rise to the formation of conductive macrocycles.[23] Enlightened by this specific property, we doped NiPc-CoTAA using iodine in an airtight vessel at 80 °C overnight. As shown in the EPR spectrum (Figure 2f), the pristine NiPc-CoTAA exhibited a series of signals with a *g* center value of 2.0048, which can be attributed to the free radical in the framework. The iodine-doped NiPc-CoTAA also showed one principal peak of free radicals at the *g* value of 2.0048, while its intensity is eight times that of pristine samples, demonstrating the greatly increased content of free radicals. The disappearance of other coupling peaks was due to sharply increased radical signal, which was overwhelming to other coupling peaks. In the Raman spectrum, the iodine-doped NiPc-CoTAA exhibited two characteristic peaks at 110, 113, and 167 cm^{-1} (Figure S17), which were assigned to the signals of symmetric I_3^- and I_5^- ions. The XPS analysis result also confirmed the content and valence of iodine in the doped NiPc-CoTAA (Figures S18–S21). In addition, the iodine-doped sample exhibited a slightly wider electronic absorption up to 1100 nm (Figure 2d). Notably, the electrical conductivity of the iodine-doped NiPc-CoTAA reached up to 0.52 $S m^{-1}$, which was approximately 64-fold improvement of its pristine counterpart and ranked as one of the highest

values among reported 2D framework materials (Table S3). Compared with other frameworks, NiPc-CoTAA is highly conductive mainly owing to several factors. Firstly, NiPc-CoTAA has a fully π-conjugated structure, which spans the 2D sheets and facilitates the migration of delocalized electrons.[22a,24a] Secondly, the phthalocyanine and cobalt tetraaza-[14]annulene units stack as columns in an eclipsed manner and offer desirable conduction pathways for charge carriers.[24b] Thirdly, the oxidation of the metal tetraaza-[14]annulene units leads to the formation of conductive macrocycles.[20,23] However, few frameworks can simultaneously satisfy all these requirements.

Film Preparation

Inspired by the high conductivity of NiPc-CoTAA, we attempted to prepare its thin films for the fabrication of high-performance sensing devices. The film was prepared using the steam-assisted conversion (VAC) approach (Figure S22), which has been reported by Medina for the preparation of highly oriented MOF thin films.[25] The NiPc[NH_2]$_8$, TMP, cobalt acetate tetrahydrate, and triethylamine were dissolved in DMF as the precursor solution. A mixture of DMF and triethylamine (20:1, v/v) was added into a vessel as the vapor source. Then an ITO substrate (1.0 cm × 1.5 cm) was placed on a platform in the vessel. A droplet of precursor solution was evenly deposited on the ITO substrate. The vessel was sealed and heated to 120 °C for 12 h. After cooling down to room temperature, the ITO substrate was taken out and washed with acetone. The NiPc-CoTAA thin films were obtained upon drying under vacuum for 1 h. Notably, the thickness of the film can be well controlled from 100 to 1000 nm by adjusting the number of droplets (Figure S23). Owing to the poor mechanical properties of NiPc-CoTAA, the thinner films (< 100 nm) are very fragile and easily to be broken into flakelets. We did not obtain the films with thickness of tens of nanometers. The wide-spread NiPc-CoTAA film was obtained with smooth, compact, and uniform surface (Figure 3a). As shown in Figure 3b, the average surface roughness was around 20 nm over an area of 5 μm × 5 μm. The high-quality film provides a reliable platform for the preparation of efficient sensor devices.

Sensing Performance for Gases

The electrical conductivity of the NiPc-CoTAA film was further measured using the current–voltage (*I–V*) method, which was carried out using an interdigitated array (IDA) Au electrode. The electrical conductivity of these films was calculated to be 6.67×10^{-3} S m^{-1}, which was nearly triple that

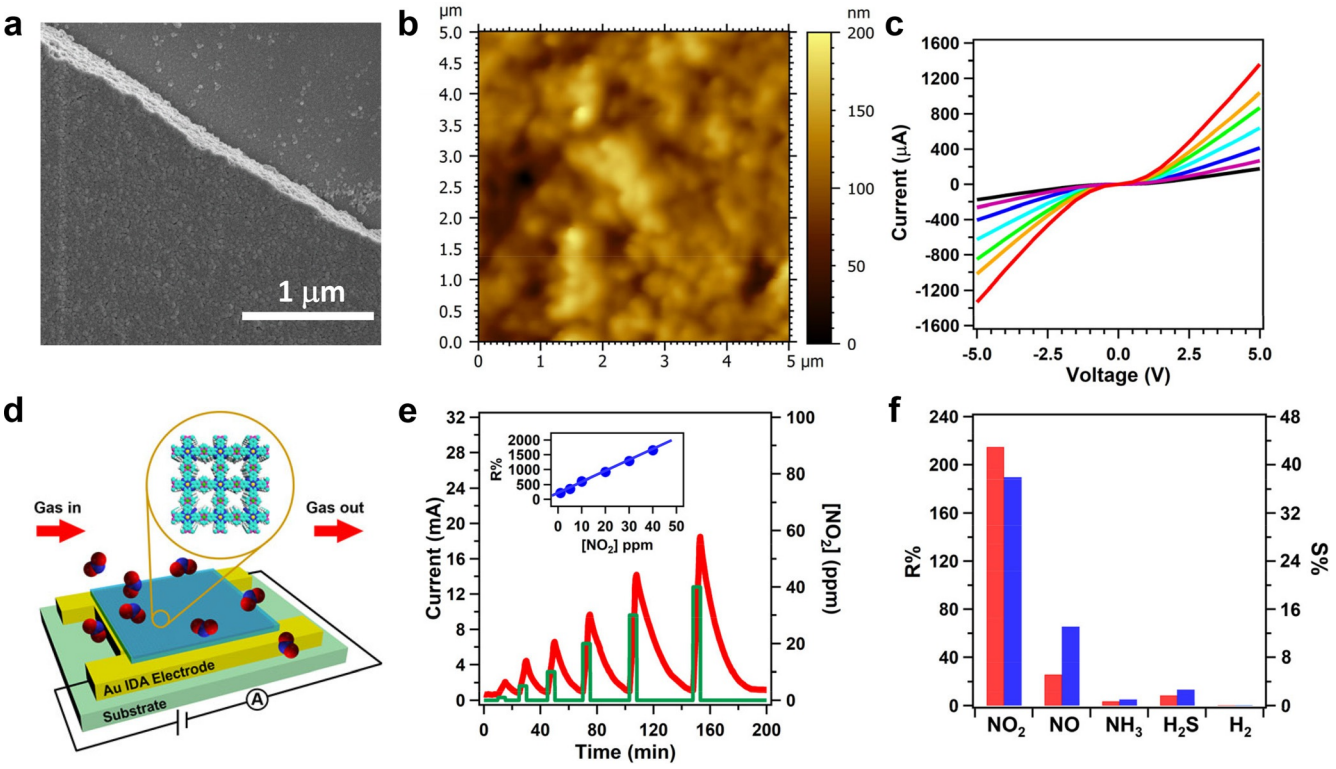

Figure 3. a) FE-SEM image of a NiPc-CoTAA thin film with a thickness of 100 nm. b) 2D AFM image of the 100 nm NiPc-CoTAA thin film. c) *I–V* curves of NiPc-CoTAA films with different thicknesses from 100 to 500 nm (black, 100 nm; purple, 150 nm; blue, 270 nm; cyan, 500 nm; green, 670 nm; orange, 800 nm; red, 1000 nm). d) Chemiresistive detection of NO_2 using NiPc-CoTAA films on a gold IDA electrode. e) Time-dependent response–recovery current plot of the 500 nm NiPc-CoTAA film at NO_2 concentrations from 1 to 40 ppm at 298 K. The inset shows the linear relation between R% and the NO_2 concentration at 298 K. f) Responsivity and sensitivity of the 500 nm NiPc-CoTAA film towards different gases (NO_2, NO, NH_3, H_2S, and H_2) at 1 ppm (red bar, R%; blue bar, S%).

of the pressed pellets owing to the more compact film nanoscale textures or higher crystal orientations. The intergrown framework crystallites could lead to more flawless tile patterns. As shown in Figure 3c, the current increase momentum was moderated along with the increase of thickness under a bias of 5.0 V, indicating the homogeneity of the films. In addition, the analysis results illustrated that the electrical conductance of the films was increased with their thickness in good linearity (Figure S24).

To investigate the possibility of utilizing the NiPc-CoTAA films for gas sensing, we prepared an electronic device with the 500 nm NiPc-CoTAA thin film (Figure 3d). Several gases, including NO_2, NO, NH_3, H_2S, and H_2 were employed as analytes to evaluate the response/recovery ability of the device. These analytes have different oxidation–reduction quality and coordination ability towards the metal centers, which could provoke a change in the electrical conductivity of NiPc-CoTAA. Upon exposure to NO_2 gas at different concentrations (1–40 ppm) at 298 K, the device exhibited different current responses. In one duty cycle, the dynamic response time was set as 5 min and the static recovery time varied from 5 to 60 min to completely release the NO_2 analyte. As shown in Figure 3e, the current intensity was increased along with the exposure time prolonging but decreased as recovery proceeded, illustrating that the p-type responsivity of NiPc-CoTAA to the oxidizing analyte. To quantitatively evaluate the responsivity (R%) at different concentrations, the percentage of current change was calculated according to the equation: $R\% = [(I_t - I_i)/I_i] \times 100\%$, where I_i represents the initial current intensity and I_t indicates the current density after exposure for 5 min to NO_2 atmosphere. The almost linear fitting curve demonstrates the interaction between NO_2 and the film is first-order kinetic (Figure 3e, inset).[26] Consequently, the concentration of NO_2 can be quantitively analyzed using the film. The R% values were calculated as 215%, 352%, 602%, 902%, 1292%, and 1658% at the NO_2 concentrations of 1, 5, 10, 20, 30, and 40 ppm, respectively. This result revealed that the NiPc-CoTAA has a superior sensitivity, which is comparable with other landmark materials, such as COF-DC-8 and UPC-H4.[22a,27] Consequently, the AA stacking mode which facilitates the orbital overlap in association of periodically crystalline and porous structures which enhances the surface area contributes to the remarkable sensing performance. In addition, the sensitivity (S%) of the film was evaluated as 37.6 ppm^{-1} using the slope of linear correlation between responsivity and the concentration of NO_2. Notably, the NiPc-CoTAA film can be recycled over five times without significant decrease in current density (Figure S25). The sensing performance of thin films with various thickness was also evaluated, while they exhibited inferior responsibility, sensitivity, and reversibility.

Inspired by the high sensing performance of NiPc-CoTAA thin films, we further studied its response/recovery behavior towards NO, NH_3, H_2S, and H_2 under the same conditions. Owing to the weaker oxidation and coordination ability of NO, the film exhibited a lower response plot with R% and S% values of 27% and 12.7% ppm^{-1} (Figure 3f, Figures S26 and S27), respectively. In contrast with the positive responses towards NO_2 and NO, the film showed a negative response when exposed to the electron-donating NH_3 and H_2S atmosphere (Figures S28–S31). The R% and S% values were calculated as 3.1% and 1.2% ppm^{-1} toward NH_3, and as 8.2% and 3.3% ppm^{-1} for H_2S, respectively. The intermolecular hydrogen bonding with nitrogen atoms in the network is possibly formed, leading to a kinetic barrier against the diffusion of these electron-donating gases. However, there was no obvious response observed for the detection of H_2 (Figure S32). The NiPc-CoTAA thin film exhibited a superior NO_2 sensing selectivity to that of NO, NH_3, H_2S, and H_2 at 298 K (Figure 3f). All these results demonstrated that the 2D NiPc-CoTAA film not only exhibited high sensitivity but also excellent selectivity as chemiresistive sensors.

Conclusion

In summary, we developed a new kind of conductive phthalocyanine-based framework material, which was connected with a conjugated tetraaza[14]annulene linkage. We unambiguously studied the crystallinity, stability, and conductivity of NiPc-CoTAA framework, with a variety of characterization methods. The high conjugation and densely stacked π-units rendered this material with a low band gap of 0.86 eV. The electrical conductivity of NiPc-CoTAA was measured as high as 8.16×10^{-3} $S\,m^{-1}$, which can be further enhanced to 0.52 $S\,m^{-1}$ after doping with iodine. The high conductivity and embedded metal phthalocyanine units makes this material promising for the detection of toxic gases. To fulfill this target, we prepared the NiPc-CoTAA thin films with tunable thicknesses from 100 to 1000 nm using the VAC method. The obtained films are of a high degree of crystal orientation and high electrical conductivity. Furthermore, the films exhibited significant sensitivity towards several redox gases. This work would constitute an important step during the development of conductive frameworks and pave the way for their applications in various practical fields.

Acknowledgements

N.H. acknowledges support by the research start-up fund of Zhejiang University. H.-C.Z. acknowledges support by the U.S. Department of Energy, Office of Science, Office of Basic Energy Sciences (DE-SC0001015), the Robert A. Welch Foundation through a Welch Endowed Chair to H.-C.Z. (A-0030), and a National Science Foundation Graduate Research Fellowship under Grant No. DGE:1252521.

Conflict of interest

The authors declare no conflict of interest.

Keywords: conducting materials · conjugated polymers · covalent organic frameworks · metal–organic frameworks · porous polymers

[1] a) O. M. Yaghi, *J. Am. Chem. Soc.* **2016**, *138*, 15507 – 15509; b) O. M. Yaghi, *Nano Lett.* **2020**, *20*, 8432 – 8434.

[2] a) H.-C. Zhou, J. R. Long, O. M. Yaghi, *Chem. Rev.* **2012**, *112*, 673 – 674; b) N. Huang, P. Wang, D. Jiang, *Nat. Rev. Mater.* **2016**, *1*, 16068.

[3] a) Y. Li, R. T. Yang, *Langmuir* **2007**, *23*, 12937 – 12944; b) A. J. Rieth, M. Dincă, *J. Am. Chem. Soc.* **2018**, *140*, 3461 – 3466; c) Y. Wang, X. Jia, H. Yang, Y. Wang, X. Chen, A. N. Hong, J. Li, X. Bu, P. Feng, *Angew. Chem. Int. Ed.* **2020**, *59*, 19027 – 19030; *Angew. Chem.* **2020**, *132*, 19189 – 19192; d) N. Huang, X. Chen, R. Krishna, D. Jiang, *Angew. Chem. Int. Ed.* **2015**, *54*, 2986 – 2990; *Angew. Chem.* **2015**, *127*, 3029 – 3033; e) N. Huang, R. Krishna, D. Jiang, *J. Am. Chem. Soc.* **2015**, *137*, 7079 – 7082.

[4] a) J. Y. S. Lin, *Science* **2016**, *353*, 121 – 122; b) R.-B. Lin, S. Xiang, H. Xing, W. Zhou, B. Chen, *Coord. Chem. Rev.* **2019**, *378*, 87 – 103; c) J.-R. Li, R. J. Kuppler, H.-C. Zhou, *Chem. Soc. Rev.* **2009**, *38*, 1477 – 1504; d) H. Fan, A. Mundstock, A. Feldhoff, A. Knebel, J. Gu, H. Meng, J. Caro, *J. Am. Chem. Soc.* **2018**, *140*, 10094 – 10098; e) S. Yuan, X. Li, J. Zhu, G. Zhang, P. V. Puyvelde, B. V. der Bruggen, *Chem. Soc. Rev.* **2019**, *48*, 2665 – 2681.

[5] a) L. Zhu, X.-Q. Liu, H.-L. Jiang, L.-B. Sun, *Chem. Rev.* **2017**, *117*, 8129 – 8176; b) A. Bavykina, N. Kolobov, I. S. Khan, J. A. Bau, A. Ramirez, J. Gascon, *Chem. Rev.* **2020**, *120*, 8468 – 8535; c) J. Guo, D. Jiang, *ACS Cent. Sci.* **2020**, *6*, 869 – 879; d) T. Kundu, J. Wang, Y. Cheng, Y. Du, Y. Qian, G. Liu, D. Zhao, *Dalton Trans.* **2018**, *47*, 13824 – 13829; e) N. Huang, K. H. Lee, Y. Yue, X. Xu, S. Irle, Q. Jiang, D. Jiang, *Angew. Chem. Int. Ed.* **2020**, *59*, 16587 – 16593; *Angew. Chem.* **2020**, *132*, 16730 – 16736.

[6] a) H.-Y. Li, S.-N. Zhao, S.-Q. Zang, J. Li, *Chem. Soc. Rev.* **2020**, *49*, 6364 – 6401; b) L. E. Kreno, K. Leong, O. K. Farha, M. Allendorf, R. P. Van Duyne, J. T. Hupp, *Chem. Rev.* **2012**, *112*, 1105 – 1125; c) Q. Gao, X. Li, G.-H. Ning, K. Leng, B. Tian, C. Liu, W. Tang, H.-S. Xu, K. P. Loh, *Chem. Commun.* **2018**, *54*, 2349 – 2352; d) Z. Li, N. Huang, K. H. Lee, Y. Feng, S. Tao, Q. Jiang, Y. Nagao, S. Irle, D. Jiang, *J. Am. Chem. Soc.* **2018**, *140*, 12374 – 12377.

[7] a) G. K. H. Shimizu, J. M. Taylor, S. Kim, *Science* **2013**, *341*, 354 – 355; b) D.-W. Lim, H. Kitagawa, *Chem. Rev.* **2020**, *120*, 8416 – 8467; c) X. Wu, Y.-L. Hong, B. Xu, Y. Nishiyama, W. Jiang, J. Zhu, G. Zhang, S. Kitagawa, S. Horike, *J. Am. Chem. Soc.* **2020**, *142*, 14357 – 14364; d) Q. Xu, S. Tao, Q. Jiang, D. Jiang, *J. Am. Chem. Soc.* **2018**, *140*, 7429 – 7432.

[8] a) Y. Zhao, X.-G. Yang, X.-M. Lu, C.-D. Yang, N.-N. Fan, Z.-T. Yang, L.-Y. Wang, L.-F. Ma, *Inorg. Chem.* **2019**, *58*, 6215 – 6221; b) Y. Cui, J. Zhang, H. He, G. Qian, *Chem. Soc. Rev.* **2018**, *47*, 5740 – 5785; c) S. Wang, X. Xu, Y. Yue, K. Yu, Q. Shui, N. Huang, H. Chen, *Small Struct.* **2020**, *1*, 2000021.

[9] a) S. Zheng, X. Li, B. Yan, Q. Hu, Y. Xu, X. Xiao, H. Xue, H. Pang, *Adv. Energy Mater.* **2017**, *7*, 1602733; b) T. Qiu, Z. Liang, W. Guo, H. Tabassum, S. Gao, R. Zou, *ACS Energy Lett.* **2020**, *5*, 520 – 532; c) S. B. Alahakoon, C. M. Thompson, G. Occhialini, R. A. Smaldone, *ChemSusChem* **2017**, *10*, 2116 – 2129; d) C. R. DeBlase, K. E. Silberstein, T.-T. Truong, H. D. Abruña, W. R. Dichtel, *J. Am. Chem. Soc.* **2013**, *135*, 16821 – 16824.

[10] a) A. V. Desai, B. Manna, A. Karmakar, A. Sahu, S. K. Ghosh, *Angew. Chem. Int. Ed.* **2016**, *55*, 7811 – 7815; *Angew. Chem.* **2016**, *128*, 7942 – 7946; b) C.-C. Wang, J.-R. Li, X.-L. Lv, Y.-Q. Zhang, G. Guo, *Energy Environ. Sci.* **2014**, *7*, 2831 – 2867; c) N. Huang, L. Zhai, H. Xu, D. Jiang, *J. Am. Chem. Soc.* **2017**, *139*, 2428 – 2434; d) N. Huang, P. Wang, M. A. Addicoat, T. Heine, D. Jiang, *Angew. Chem. Int. Ed.* **2017**, *56*, 4982 – 4986; *Angew. Chem.* **2017**, *129*, 5064 – 5068.

[11] a) N. Huang, K. Wang, H. Drake, P. Cai, J. Pang, J. Li, S. Che, L. Huang, Q. Wang, H.-C. Zhou, *J. Am. Chem. Soc.* **2018**, *140*, 6383 – 6390; b) N. Huang, S. Yuan, H. Drake, X. Yang, J. Pang, J. Qin, J. Li, Y. Zhang, Q. Wang, D. Jiang, H.-C. Zhou, *J. Am. Chem. Soc.* **2017**, *139*, 18590 – 18597; c) X. Xu, S. Wang, Y. Yue, N. Huang, *ACS Appl. Mater. Interfaces* **2020**, *12*, 37427 – 37434; d) J.-L. Shi, R. Chen, H. Hao, C. Wang, X. Lang, *Angew. Chem. Int. Ed.* **2020**, *59*, 9088 – 9093; *Angew. Chem.* **2020**, *132*, 9173 – 9178.

[12] a) J. Li, Y. Fan, Y. Ren, Y. Liao, C. Qi, H. Jiang, *Inorg. Chem.* **2018**, *57*, 1203 – 1212; b) M. H. Beyzavi, R. C. Klet, S. Tussupbayev, J. Borycz, N. A. Vermeulen, C. J. Cramer, J. F. Stoddart, J. T. Hupp, O. K. Farha, *J. Am. Chem. Soc.* **2014**, *136*, 15861 – 15864; c) L.-H. Li, X.-L. Feng, X.-H. Cui, Y.-X. Ma, S.-Y. Ding, W. Wang, *J. Am. Chem. Soc.* **2017**, *139*, 6042 – 6045; d) S. Yan, X. Guan, H. Li, D. Li, M. Xue, Y. Yan, V. Valtchev, S. Qiu, Q. Fang, *J. Am. Chem. Soc.* **2019**, *141*, 2920 – 2924.

[13] a) T. Sawano, N. C. Thacker, Z. Lin, A. R. McIsaac, W. Lin, *J. Am. Chem. Soc.* **2015**, *137*, 12241 – 12248; b) M. J. Kalmutzki, N. Hanikel, O. M. Yaghi, *Sci. Adv.* **2018**, *4*, eaat9180.

[14] a) C. Kutzscher, G. Nickerl, I. Senkovska, V. Bon, S. Kaskel, *Chem. Mater.* **2016**, *28*, 2573 – 2580; b) V. Pascanu, G. G. Miera, A. K. Inge, B. Martín-Matute, *J. Am. Chem. Soc.* **2019**, *141*, 7223 – 7234; c) H. Xu, J. Gao, D. Jiang, *Nat. Chem.* **2015**, *7*, 905 – 912.

[15] a) T. M. Swager, K. A. Mirica, *Chem. Rev.* **2019**, *119*, 1 – 2; b) M. Ko, L. Mendecki, K. A. Mirica, *Chem. Commun.* **2018**, *54*, 7873 – 7891; c) U. Lange, V. M. Mirsky, *Anal. Chim. Acta* **2011**, *687*, 105 – 113; d) W.-T. Koo, J.-S. Jang, I.-D. Kim, *Chem* **2019**, *5*, 1938 – 1963.

[16] a) L. Sun, M. G. Campbell, M. Dincă, *Angew. Chem. Int. Ed.* **2016**, *55*, 3566 – 3579; *Angew. Chem.* **2016**, *128*, 3628 – 3642; b) L. S. Xie, G. Skorupskii, M. Dincă, *Chem. Rev.* **2020**, *120*, 8536 – 8580.

[17] a) H.-C. Zhou, S. Kitagawa, *Chem. Soc. Rev.* **2014**, *43*, 5415 – 5418; b) H. Furukawa, K. E. Cordova, M. O'Keeffe, O. M. Yaghi, *Science* **2013**, *341*, 1230444; c) S. J. Lyle, P. J. Waller, O. M. Yaghi, *Trends Chem.* **2019**, *1*, 172 – 184.

[18] a) M. G. Campbell, D. Sheberla, S. F. Liu, T. M. Swager, M. Dincă, *Angew. Chem. Int. Ed.* **2015**, *54*, 4349 – 4352; *Angew. Chem.* **2015**, *127*, 4423 – 4426; b) E. M. Miner, T. Fukushima, D. Sheberla, L. Sun, Y. Surendranath, M. Dincă, *Nat. Commun.* **2016**, *7*, 10942; c) I. Stassen, J.-H. Dou, C. Hendon, M. Dincă, *ACS Cent. Sci.* **2019**, *5*, 1425 – 1431.

[19] a) X. Ding, L. Chen, Y. Honsho, X. Feng, O. Saengsawang, J. Guo, A. Saeki, S. Seki, S. Irle, S. Nagase, V. Parasuk, D. Jiang, *J. Am. Chem. Soc.* **2011**, *133*, 14510 – 14513; b) S. Jin, M. Supur, M. Addicoat, K. Furukawa, L. Chen, T. Nakamura, S. Fukuzumi, S. Irle, D. Jiang, *J. Am. Chem. Soc.* **2015**, *137*, 7817 – 7827; c) X. Feng, L. Chen, Y. Honsho, O. Saengsawang, L. Liu, L. Wang, A. Saeki, S. Irle, S. Seki, Y. Dong, D. Jiang, *Adv. Mater.* **2012**, *24*, 3026 – 3031.

[20] Y. Jiang, I. Oh, S. H. Joo, O. Buyukcakir, X. Chen, S. H. Lee, M. Huang, W. K. Seong, S. K. Kwak, J.-W. Yoo, R. S. Ruoff, *J. Am. Chem. Soc.* **2019**, *141*, 16884 – 16893.

[21] a) F. I. Bohrer, C. N. Colesniuc, J. Park, M. E. Ruidiaz, I. K. Schuller, A. C. Kummel, W. C. Trogler, *J. Am. Chem. Soc.* **2009**, *131*, 478 – 485; b) F. I. Bohrer, C. N. Colesniuc, J. Park, I. K. Schuller, A. C. Kummel, W. C. Trogler, *J. Am. Chem. Soc.* **2008**, *130*, 3712 – 3713; c) K.-C. Ho, Y.-H. Tsou, *Sens. Actuators B* **2001**, *77*, 253 – 259; d) C. J. Liu, J. J. Shih, Y. H. Ju, *Sens. Actuators B* **2004**, *99*, 344 – 349.

[22] a) Z. Meng, R. M. Stolz, K. A. Mirica, *J. Am. Chem. Soc.* **2019**, *141*, 11929 – 11937; b) M.-D. Zhang, D.-H. Si, J.-D. Yi, S.-S. Zhao, Y.-B. Huang, R. Cao, *Small* **2020**, *16*, 2005254.

[23] a) P. J. Spellane, L. V. Interrante, R. K. Kullnig, F. S. Tham, *Inorg. Chem.* **1989**, *28*, 1587 – 1590; b) A. M. Whyte, Y. Shuku, G. S. Nichol, M. M. Matsushita, K. Awaga, N. Robertson, *J. Mater. Chem.* **2012**, *22*, 17967.

[24] a) J. Guo, Y. Xu, S. Jin, L. Chen, T. Kaji, Y. Honsho, M. A. Addicoat, J. Kim, A. Saeki, H. Ihee, S. Seki, S. Irle, M. Hiramoto, J. Gao, D. Jiang, *Nat. Commun.* **2013**, *4*, 2736; b) X. Feng, L. Liu, Y. Honsho, A. Saeki, S. Seki, S. Irle, Y. Dong, A. Nagai, D. Jiang, *Angew. Chem. Int. Ed.* **2012**, *51*, 2618 – 2622; *Angew. Chem.* **2012**, *124*, 2672 – 2676.

[25] E. Virmani, J. M. Rotter, A. Mähringer, T. von Zons, A. Godt, T. Bein, S. Wuttke, D. D. Medina, *J. Am. Chem. Soc.* **2018**, *140*, 4812 – 4819.

[26] F. I. Bohrer, A. Sharoni, C. Colesniuc, J. Park, I. K. Schuller, A. C. Kummel, W. C. Trogler, *J. Am. Chem. Soc.* **2007**, *129*, 5640 – 5646.

[27] Y. Wang, D. Liu, J. Yin, Y. Shang, J. Du, Z. Kang, R. Wang, Y. Chen, D. Sun, J. Jiang, *Chem. Commun.* **2020**, *56*, 703 – 706.

Manuscript received: January 16, 2021
Accepted manuscript online: February 26, 2021
Version of record online: April 1, 2021

